pH-Sensitive Tubular Polymersomes: Formation and Applications in Cellular Delivery

James D. Robertson,[†,‡,§,∥,⊥] Guy Yealland,[†,‡,§,⊥,#,⊗] Milagros Avila-Olias,[†,‡,§] Luca Chierico,[†,‡] Oliver Bandmann,[⊥,#,⊗] Stephen A Renshaw,[∥,⊥] and Giuseppe Battaglia[†,‡,*]

[†]Department of Chemistry, [‡]The MRC/UCL Centre for Molecular and Medical Virology, University College London, London, United Kingdom and [§]Department of Biomedical Science, [∥]Department of Infection and Immunity, [⊥]MRC Centre for Developmental and Biomedical Genetics, [#]Department of Neuroscience, and [⊗]Sheffield Institute of Translational Neuroscience, University of Sheffield, Sheffield, United Kingdom

ABSTRACT Optimizing the shape of a nanovector influences its interaction with a cell and determines the internalization kinetics. Block copolymer amphiphiles self-assemble into monodisperse structures in aqueous solutions and have been explored extensively as drug delivery vectors. However, the structure of self-assembled block copolymers has mainly been limited to spherical vesicles or spherical and worm-like micelles. Here we show the controlled formation and purification of tubular polymersomes, long cylindrical vesicles. Tubular polymersomes are purified from other structures, and their formation is manipulated by incorporating the biocompatible membrane components cholesterol and phospholipids. Finally we show that these tubular polymersomes have different cellular internalization kinetics compared with spherical polymersomes and can successfully encapsulate and deliver fluorescent bovine serum albumin protein intracellularly.

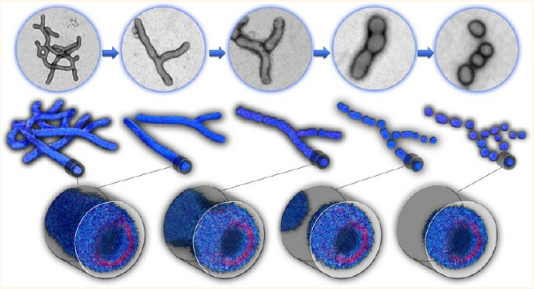

KEYWORDS: tubular polymersomes · polymersomes · nanotubes · drug delivery · endocytosis

When designing nanoscopic vectors, the ability to facilitate cellular delivery is a particularly desirable quality. The creation of nanoparticles able to bypass cellular barriers and deliver cargo within the cell has enabled new therapeutic and diagnostic approaches.[1−3] The most typical approach is to target the cell endocytosis machinery, an energy-dependent intake mechanism in eukaryotic cells. During endocytosis material is internalized into intracellular vesicles, which are then transported into a network of endocytic organelles where the materials are sorted and metabolized.[4] The mechanism of endocytosis is dependent on the nature of receptor(s) targeted, the cell type, and the cargo size.[4] It has been shown that by controlling nanoparticle parameters such as the size, shape, surface chemistry, and surface topology it is possible to manipulate the endocytosis machinery to initiate and influence the rate of internalization. For rod-shaped nanovectors, high aspect ratios have reduced internalization in certain cell types, and long cylindrical nanovectors have shown improved circulation times and cell targeting capability.[5−9]

The ability of block copolymer amphiphiles to self-assemble into nanoparticles upon hydration has attracted interest in the field of drug delivery. Block copolymer micelles and vesicles, also known as polymersomes, offer several advantages over other nanovectors. When designing a block copolymer, it is possible to control the shape and surface chemistry of the self-assembled nanoparticle.[1] Polymersomes can encapsulate hydrophobic molecules within their membrane, but unlike solid nanoparticles, polymersomes are also capable of encapsulating a range of hydrophilic drugs, biomolecules, and even smaller nanoparticles within their lumen.[10]

In recent years we have reported the use of pH-sensitive polymersomes from the copolymer poly(2-(methacryloyloxy)ethylphosphorylcholine)-*co*-poly(2-(diisopropylamino)-ethyl methacrylate) (PMPC−PDPA) that assemble and dissemble around the endocytic

* Address correspondence to g.battaglia@ucl.ac.uk,.

Received for review January 21, 2014 and accepted April 11, 2014.

Published online April 11, 2014
10.1021/nn5004088

pH (pH = 6.2). Once internalized, the polymersomes are trafficked to an early endosome, where the pH is lowered through a controlled ion flux across the endosomal membrane. The lowered pH initiates the disassembly of the polymersome and release of its cargo. A sudden increase in cationic polymer chains within the endosome causes a rise in osmotic pressure, which temporarily destabilizes the endosomal membrane, allowing passage of the cargo into the rest of the cell. We have demonstrated that this approach can be used for the cellular delivery of DNA,[11,12] proteins,[13] anticancer drugs,[14] and antibiotics,[15] as well as several probes.[10,16] We have also shown that the polymersome size and surface topology affect the rate of internalization.[17] Here we expand our studies, reporting the formation of pH-sensitive tubular polymersomes from polymer film hydration and their isolation by sequential centrifugation. We incorporate the biological membrane components cholesterol and phospholipids to explore their effect on tubular polymersome formation and stabilization. Finally we show that these tubular polymersomes can encapsulate proteins and deliver their cargo into clinically relevant cells with the kinetics of endocytosis strongly influenced by their shape.

RESULTS AND DISCUSSION

Formation of Tubular Polymersomes. Amphiphilic copolymers with dimensionless packing parameters larger than 0.5 form membranes, which are most stable wrapped as vesicles.[18] The final polymersome shape, as for any other vesicle, is the result of the combination of forces that control the membrane wrapping and the distribution of the molecules between the inner and outer monolayers. This distribution is fixed at the time of membrane closure and generally varies widely from vesicle to vesicle. This means that vesicles can close into a great variety of morphologies, with the spherical shape being the most stable and thus most common. In polymersomes, the high viscosity of the membrane gives it a limited lateral mobility,[19] which can hinder molecular rearrangements necessary to stabilize spherical vesicles. This often drives the formation of metastable structures whose lifetimes are considerably longer than small amphiphile vesicles.[20] Without any further energy contribution to homogenize the dispersion, often spherical vesicles and nonspherical vesicles coexist.[21,22] This means the way that polymersomes are formed inherently affects their final shape. Several groups have reported the formation of tubular polymersomes using a number of approaches, but are often unstable, require complex manipulation, are formed in a nonbiocompatible solvent, or have not been isolated from contaminating spherical polymersomes.[22−25] More recently it was shown that polymersomes could be elongated by the addition of a cross-linker. It is believed the cross-linker alters the differential area between the two monolayers that form the membrane, which leads to an elongation of the vesicle.[26] However, such an approach induces chemical cross-linking and hence strips the polymersomes of their supramolecular nature.

To explore the morphology of $PMPC_{25}$−$PDPA_{65}$ assemblies using different methods of formation, polymersomes were made using pH switch or film rehydration. In the former the PMPC−PDPA copolymers are initially solubilized in low-pH phosphate-buffered saline (PBS), and their self-assembly is then controlled by raising to physiological pH (7.4). In film rehydration, the polymersome formation is achieved by solvent casting a thin copolymer film and placing the film in contact with a PBS solution under vigorous stirring for several weeks. Polymersomes gradually bud from the interface between the water and the solid film. Figure 1a shows the structure of self-assembled PMPC−PDPA aggregates formed using pH switch (left image) or film rehydration methods (right image). Self-assembly through the pH switch method resulted in the production of mostly spherical polymersomes,[27] whereas film rehydration formed a mixture of spherical and tubular polymersomes. Both dispersions have a clear vesicular nature, as evident from the size and typical deflated ball morphology shown by the TEM. This was further confirmed by small-angle X-ray scattering (SAXS), where both patterns for the pH switch and film rehydration show the typical form-factor expected of vesicles (supplementary Figure 1a).

To further understand the difference in polymersome formation using these two approaches, the PMPC−PDPA film rehydration was monitored *in situ* by confocal imaging of a rhodamine 6G-conjugated PMPC−PDPA film placed on a glass coverslip at a 90° angle to the lens. At time 0 h, aqueous PBS was added to the film and left agitating with a magnetic stirrer (Figure 1b). Like other spinodal processes, the surface of the smooth film becomes unstable, and perturbations from thermal and mechanical fluctuations induce pressure gradients across the film.[28] Oscillations in the film produce regions of increased thickness, which heightens local disjoining pressure, leading to perforations and initiating the process of dewetting. As the film begins to hydrate and swell, the membrane wrinkles and the simultaneous diffusion of the solvent toward the film and the film toward the solvent leads to fingering instabilities (Figure 1b, 2 h).[29] As the holes grow, the accumulation of polymer from these holes leads to characteristic rims developing at the periphery (Figure 1b, 20 h).[30] After 40 h these rims expand and coalesce, forming a bicontinuous network. In other studies of block copolymer dewetting, bicontinuous structures will then break up into droplets or bud off the film as vesicles.[31,32] We show that the mechanical shear stress from magnetic stirring can break off parts of the bicontinuous network before it dewets further into droplets (Figure 1b 40 h). The size of the breakages

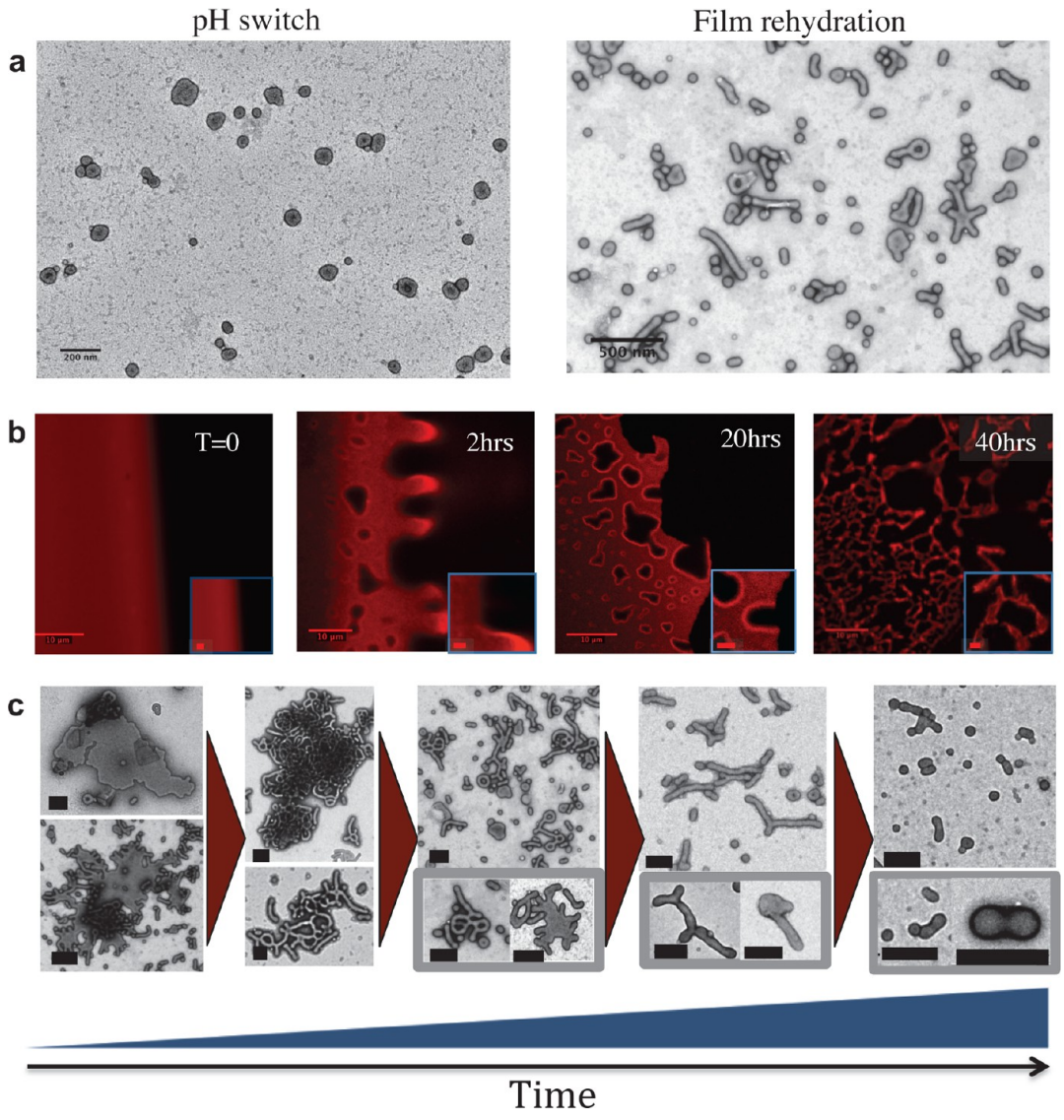

Figure 1. Formation of tubular polymersomes from a thin film. (a) TEM microscopy showing the morphology of the self-assembled block copolymer PMPC–PDPA by two methods: pH switch, as shown in the left image, and thin film rehydration on the right. (b) Dewetting of a thin film of polymer conjugated to rhodamine 6G and imaged using scanning confocal microscopy. At time 0 h PBS was added and the film was left with a magnetic stirrer. The film swells, develops holes that expand, and finally forms a bicontinuous network that breaks off into the solution. Zoomed-in inset scale bar is 2 μm. (c) Released pieces of film swell into a continuous tubular network; this then breaks into single tubes and small entangled structures. These break further into smaller tubes that finally pearl and bud into spherical polymersomes; the scale bar represents 200 nm.

released from the film varied from less than a micrometer to tens of micrometers in length (supplementary Figure 1b).

We have shown previously that as the water diffuses into the polymer film lyotropic phases begin to form with an architecture controlled by the copolymer/water ratio.[21,33] Once detached from the film, the local polymer concentration drops, favoring the formation of separated isotropic structures. Lyotropic crystals are predominantly maintained through a combination of van der Waals forces and the hydrophobic interaction, which depend on the local concentration.[34] The strong repulsive forces from hydration overcome van der Waals forces, and the edges and membrane fluctuations promote bending of the membrane into hollow enclosed structures.[35] This process was observed through transmission electron microscopy (TEM) (Figure 1c). In a similar manner to the bulk film, small breakages begin to swell and develop holes, leading to a connected tubular network. The combination of energy provided by the stirring and the repulsive hydration forces promotes the detachment of smaller branched tubular structures and diverse high-genus assemblies (supplementary Figure 1c). These particles then break up into tubular polymersomes. Finally, through processes of pearling and budding, these tubes break further into smaller tubes and finally spherical polymersomes (Figure 1c).

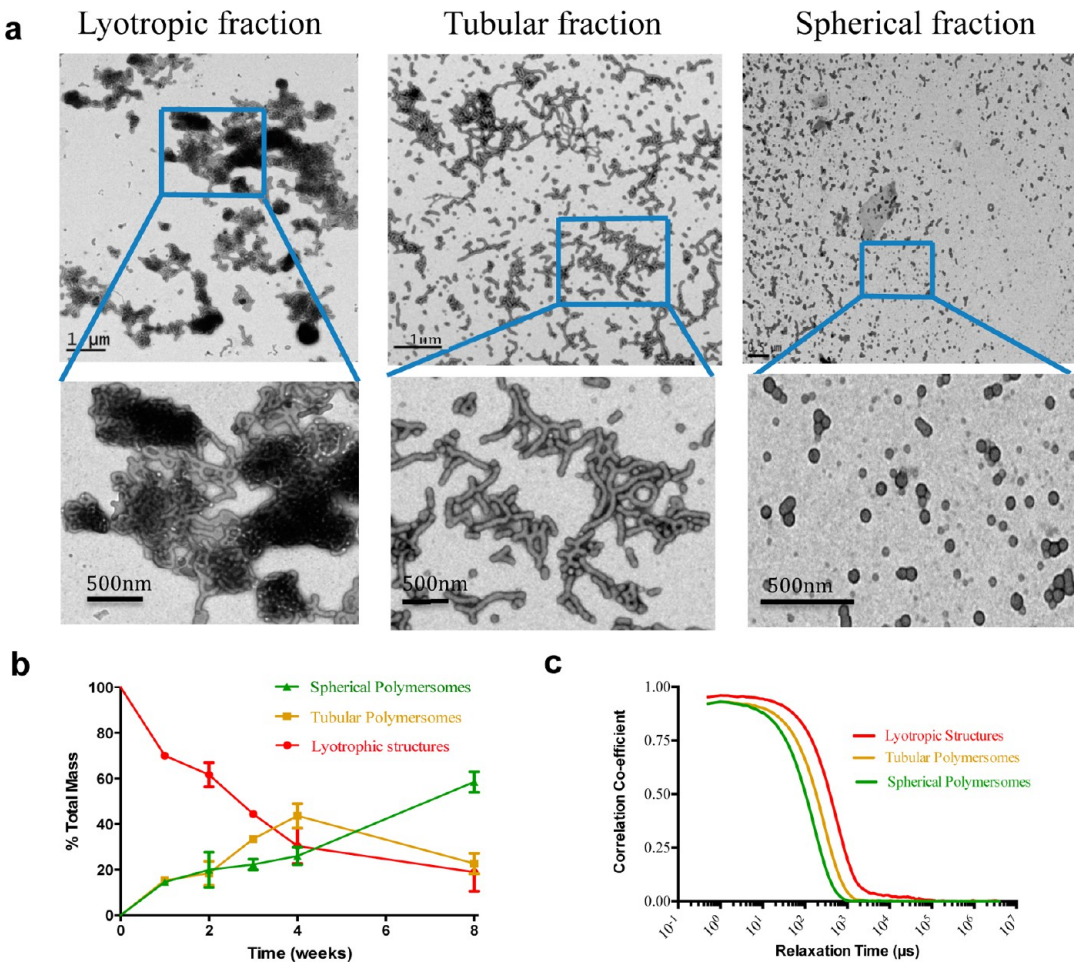

Figure 2. Separation of self-assembled structures by centrifugation. (a) The sample was spun at 2000 RCF, and the pellet was resuspended; this fraction contained the lyotropic structure shown in the image on the left. The leftover supernatant was then centrifuged at 15 000 RCF, and the pellet resuspended; this contained the tubular fraction shown in the central micrograph. The leftover supernatant contained the predominately spherical fraction, as shown in the micrograph on the right. (b) Percentage of structures over time as measured using HPLC with UV detection. (c) Correlation coefficient of the three separated fractions as measured by DLS. Error bars represent the standard deviation of three vials.

Sections of the swollen film are continuously released until the film has been discharged into the solution. This means at any one time multiple phases in the transition will coexist. In order to purify the tubular polymersomes from the other structures, the samples were centrifuged at two speeds, separating the particles based on their size and density (Figure 2a). First, the sample was centrifuged at 2000 RCF (rotational centrifugal force), and the pellet was removed and resuspended. This fraction contained the large particles from the lyotropic phases. The supernatant was then recentrifuged at 15 000 RCF, and the pellet was removed and resuspended. This fraction contained the tubular polymersomes. Those particles that remained in the supernatant were the third fraction, containing predominantly smaller, spherical particles. By separating the solution into these three fractions it was possible to quantify the relative mass of each fraction using HPLC with UV detection (Figure 2b). In keeping with the model of formation, the lyotropic structures initially form a high percentage of detached particles. Over time, these begin to disassemble, and the number of tubular and spherical polymersomes increases. At week 4 the number of tubular polymersomes reaches its maximum and then decreases, while the amount of spherical polymersomes continues to increase. This maximum signifies the point at which the transition of tubular polymersomes into spherical polymersomes overtakes the number of tubular polymersomes formed from the lyotropic structures, as the lyotropic fraction is depleted. The correlation function for the three separated fractions as measured by dynamic light scattering (DLS) is shown in Figure 2c, and a histogram of the size distribution can be found in supplementary Figure 1d.

Phospholipids and Cholesterol Alter the Transition Pathway. The effect of altering the composition of plasma membrane phospholipids, proteins, and cholesterol has been studied in great detail.[36,37] Mixing these molecules in different combinations can be used to control the membrane curvature and fluidity. To explore this in our synthetic membrane, known concentrations of phospholipid 1-palmitoyl-2-oleoyl-*sn*-glycero-3-phosphocholine

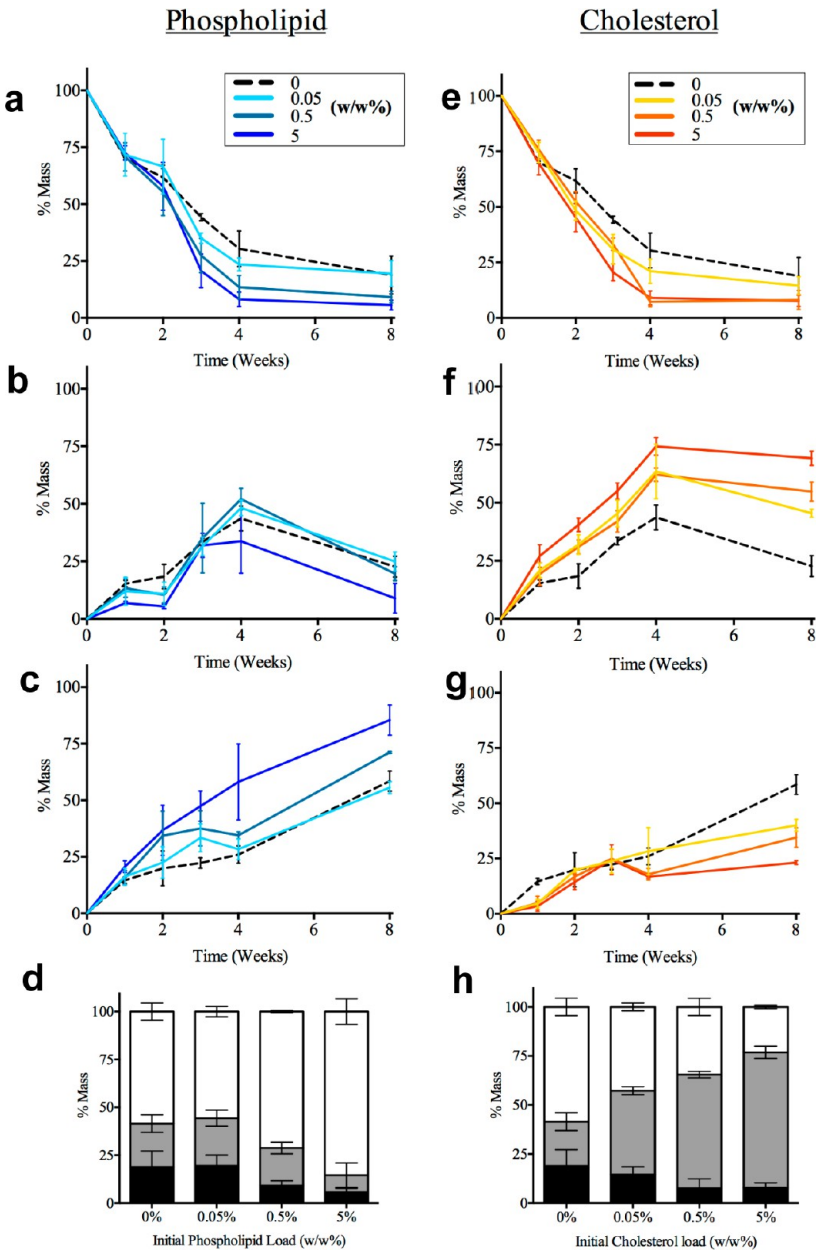

Figure 3. A phospholipid and cholesterol alter the transition of structures over time. The effect of a phosphocholine-based lipid (PC) and cholesterol (Chol) on the number of spherical, tubular, and lyotropic structures was assessed by quantifying the relative mass of each centrifugally separated fraction over time, using HPLC with UV detection. Line graphs are plotted showing the percent of spherical polymersomes (a, e), tubular polymersomes (b, f), and lyotropic structures (c, g) with the addition of 0.05%, 0.5%, or 5% PC (left) or Chol (right). (d and h) Relative proportions of the spherical polymersomes (white bars), tubular polymersomes (gray bars), or lyotropic structures (black bars) after 8 weeks of stirring with the addition of PC or Chol, respectively. Error bars represent the standard deviation of three repeats.

(PC) were added to introduce local defects in the polymersome membrane favoring curved structures. Similarly, this was repeated with the addition of cholesterol to explore the effect of membrane fluidity on the transition from tubes to spheres. Polymer films were formed with the addition of 0.05%, 0.5%, and 5% (w/w) cholesterol or PC and hydrated following the same thin film rehydration protocol. Samples of each were taken at defined intervals, fractioned, and quantified as described above (Figure 3 and supplementary Figure 2). The addition of PC or cholesterol resulted in a faster transition from larger lyotropic structures to isotropic structures in a manner proportional to load (Figure 3c,g). Interestingly, while addition of PC favored an increased formation of spherical polymersomes, the addition of cholesterol increased the proportion of tubular polymersomes over time compared with the control (Figure 3a,b,e,f). As described above, the transition from tubular polymersomes to spherical polymersomes requires the membrane to undergo pearling, a process where parts of the membrane pinch toward one another (Figure 1c). While the membrane

curvature of $PMPC_{25}-PDPA_{65}$ favors the formation of spherical polymersomes, pearling demands the membrane to bend close together, for which there is a high-energy demand. It has been observed that lipids mixed with block copolymers form lipid-rich domains on the membrane.[38,39] These domains will provide regions in the tubular polymersome with high fluidity, promoting local pearling and budding into smaller tubes or spherical polymersomes.

In contrast, cholesterol-loaded particles demonstrate a marked increase in the percentage of tubular polymersomes (Figure 3h), and the percentage of spherical polymersomes compared with the control is considerably lower (Figure 3a,d). This suggests cholesterol is stabilizing the tubular polymersomes and preventing their transition into spherical polymersomes. These results are in agreement with a recent study by Winzen and colleagues, who investigated the effect of additional cholesterol or a phosphocholine-based lipid on the mechanical properties of polymersomes formed from the block copolymer poly(dimethylsiloxane)-*block*-poly(2-methyloxazoline) (PDMS-*b*-PMOXA).[40] They found the addition of the lipid produced vesicles with similar packing densities to the control polymersomes, whereas cholesterol interacted strongly with the polymer, resulting in a considerably higher packing density. This meant that the Young's modulus and bending modulus were significantly greater; hence the membrane had an increased bending stiffness and improved mechanical stability.[40] When interpreted in this context, our data suggest that the improved mechanical stability of the cholesterol membrane results in a stabilization of the tubular polymersomes and a slower progression to spherical structures. The fact that cholesterol also eases the transition from lyotropic to isotropic structures might also result from an increased packing density, where membranes are more readily stabilized.

Following 8 weeks' formation the morphology of tubular polymersomes was further studied through analysis of electron micrographs. Representative micrographs of each group can be seen in Figure 4a. The persistent length and total length of at least 500 tubular polymersomes in each group were measured and plotted on a histogram as a percentage of the number of particles or as a percentage of the number of polymer chains (*N*(agg)) (Figure 4b). Particles encapsulating 5% PC were on average shorter than those of the other two groups. This is consistent with the notion that the PC speeds up the pearling process. The persistent length and total length of the cholesterol and control group were similar. In Figure 4c tubular polymersomes are organized by branch number (Figure 4c). The mean number of branches was lower than the control for the PC group and higher for the cholesterol group. These results are in keeping with the additives' roles in fluidizing and stabilizing the membrane.

Investigating the Potential of Tubular Polymersomes as Intracellular Delivery Vectors. The uptake kinetics of tubular polymersomes was investigated in primary human neutrophils and FaDu cells. FaDu cells are an adherent epithelial cell line established from the pharynx of a patient with squamous cell carcinoma, while neutrophils are a nonadherent blood leukocyte. Cancer cells and immune cells are among the most well studied in drug delivery. Nanovectors are often sought to improve the selectivity and efficiency of chemotherapeutics in cancer therapy, and immune cells are highly relevant as both an obstacle and a target in drug delivery.[41,42]

Neutrophils are the most numerous leukocyte in the blood and play a key role in the elimination of foreign bodies through phagocytosis. In addition, neutrophils are major effector cells in acute inflammation and have been subjected to much research for the treatment of crippling disorders such as rheumatoid arthritis and chronic obstructive pulmonary disease. Yet these cells have been largely ignored in nanotechnology, as they have proven difficult to work with due to their short lifespans and susceptibility to immune activation.

To compare the internalization kinetics of tubular polymersomes with spherical polymersomes, flow cytometry was used to quantify the uptake of these particles into neutrophils and FaDu cells over time. To ensure that any difference between the spherical and tubular particles is a result of shape rather than size, the mean diameters of the spherical polymersomes were designed to mimic the diameter and the length of the tubular polymersomes: 60 and 240 nm, respectively (supplementary Figure 3). The fluorescence intensity in each group was normalized by the mass of polymer per particle so that the final value was proportional to the number of particles internalized as opposed to the amount of polymer. A biphasic uptake profile was observed for the tubes in both cell types (Figure 5a). The uptake profile is different from that observed for the spherical polymersomes, which show a rapid internalization followed by a single plateau.[27] The two-phase increase in fluorescence for cells incubated with tubular particles can be explained by an initial quick binding step, followed by a slow internalization. Confocal microscopy reveals a predominant cell membrane localization after a 5 h incubation, whereas after 9 h the rhodamine signal can be seen within the cells, signifying successful internalization (Figure 5b, supplementary Figures 4, 5). In contrast fluorescence can be clearly observed within neutrophils after just 5 h of incubation with rhodamine-labeled spherical polymersomes (Figure 5d).

In order to explore tubular polymersomes as a drug delivery vector, we encapsulated fluorescent BSA using electroporation (see Figure 5c left image).[43] Following purification the encapsulation efficiency was

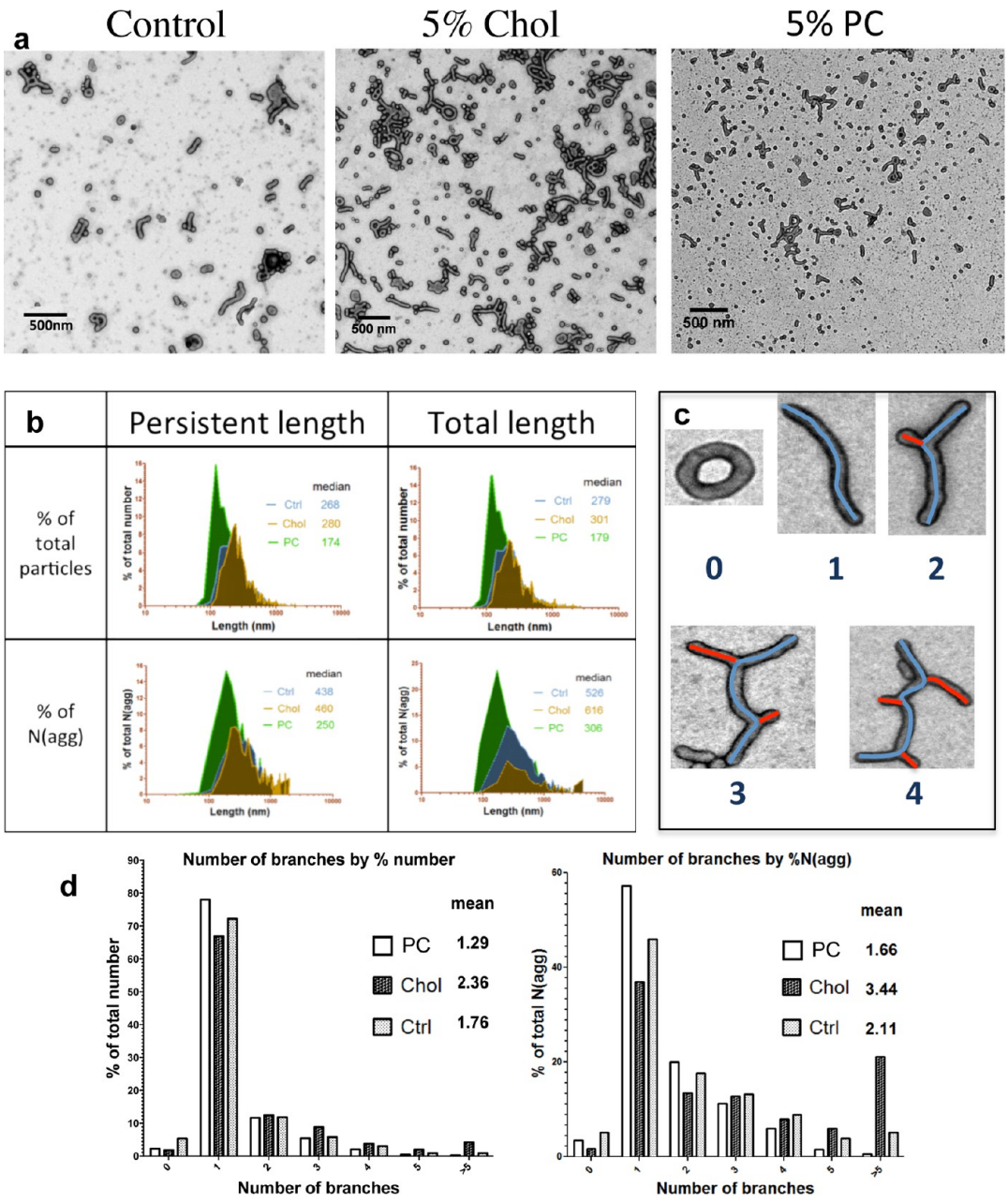

Figure 4. TEM analysis of tubular polymersomes formed after 8 weeks. (a) Representative TEM micrographs of particles formed after 8 weeks of film rehydration with mechanical stirring. (b) Image analysis of TEM micrographs showing the distribution of the persistent length and total length of tubular polymersomes, showing the control (Ctrl) or tubular polymersomes formed with the addition of 5% cholesterol (Chol) or the phosphocholine lipid (PC). The data are normalized as a percentage of the total number of tubular particles or as a percentage of the number of polymer chains (*N*(agg)) in all the tubular polymersomes. (c) Examples of increasingly branched tubular polymersomes with the branch number highlighted below each image. (d) Analysis of the number of branches formed from tubular polymersomes in the three groups. The data are normalized by the percentage of particles (left) or the percentage of the total *N*(agg) (right).

determined to be 29% by fluorescence spectroscopy, a value higher than previously observed with spherical polymersomes.[43] These tubular polymersomes were then incubated with neutrophils (Figure 5c central) or FaDu cells (Figure 5c, right) for 9 h before imaging with a confocal microscope. Single *z*-plane images demonstrate the successful intracellular delivery of BSA (Figure 5c).

3D analysis of confocal *z* slices was conducted for single neutrophils treated with the rhodamine-labeled tubular polymersomes (Figure 6a) for 5 h (Figure 6c) or 9 h (Figure 6d). The neutrophil is displayed from two angles: facing the neutrophil (Figure 6c,d left image) or looking at the neutrophil from the side (Figure 6c,d central image). The image on the right shows a single *x* slice through the center. At both time points tubular polymersomes can be seen on the membrane of the cell; however, after 9 h tubular structures can also be seen within the cell. Interestingly, fully mature endosomes reach no greater than 500 nm in diameter. If

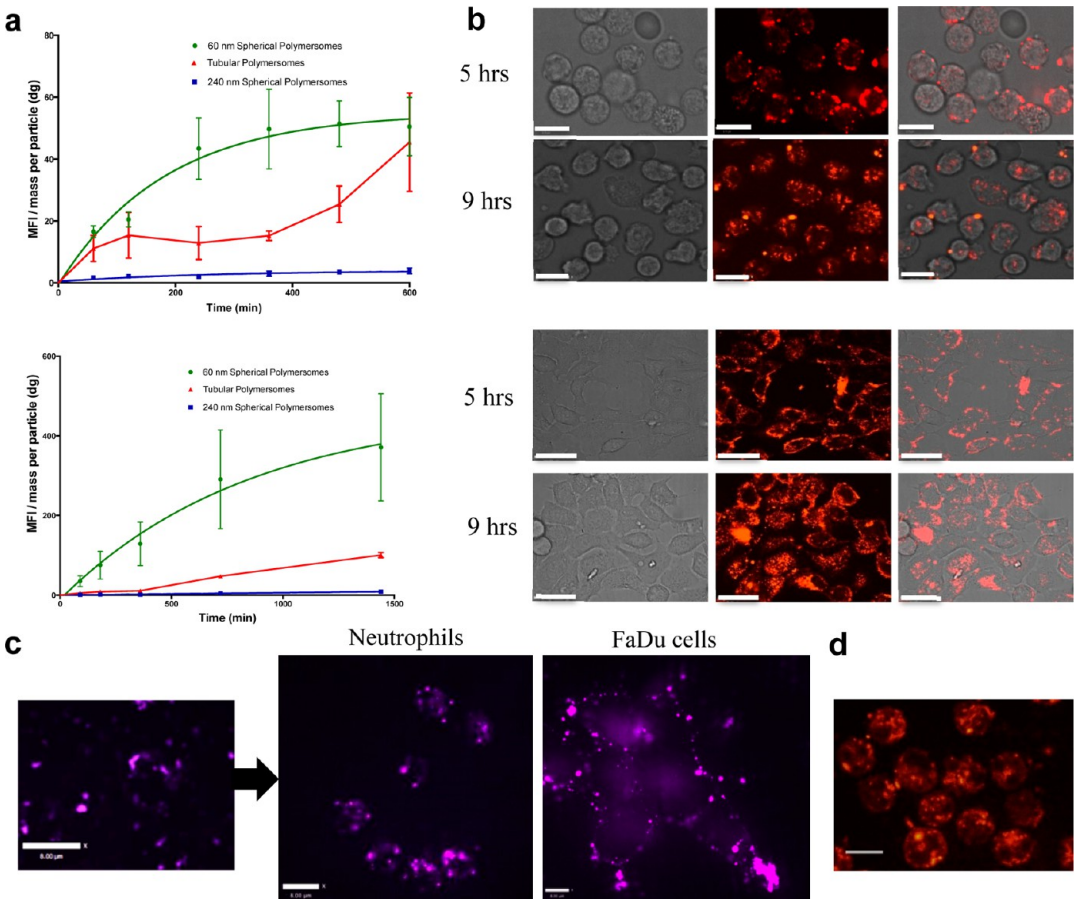

Figure 5. Internalization of tubular polymersomes into primary human neutrophils and FaDu cells. (a) Using flow cytometry, the rate of uptake of rhodamine-conjugated tubular polymersomes was measured in primary human neutrophils (top image) and FaDu cells (lower image). The internalization displays a two-phase kinetics profile. The initial increase in fluorescence corresponds to the binding of the tubular polymersomes; the second stage corresponds to the delayed internalization event. In contrast spherical polymersomes are internalized rapidly (green graphs). The data are given for the median fluorescence intensity (MFI) normalized by the mass per particle (dg). (b) Binding and internalization events visualized using confocal microscopy. At 5 h the tubular polymersomes are predominantly found on the membrane of the neutrophils (top image) and FaDu cells (lower image). After 9 h a large proportion of the fluorescent polymer can be visualized within the cells. Scale bar represents 5 μm for neutrophils and 40 μm for FaDu cells. (c) Fluorescent BSA encapsulated within tubular polymersomes using electroporation. A micrograph of the tubular polymersomes is shown on the left. The tubular polymersomes were then incubated with neutrophils (central image) or FaDu cells (right image) for 9 h before confocal microscopy. Micrographs are shown for a single *z* slice of representative cell populations. Scale bar is 8 μm. (d) Neutrophils treated for 5 h with rhodamine-labeled spherical polymersomes; scale bar is 8 μm.

tubular polymersomes with a length greater than 500 nm are internalized, they may be sorted through a different pathway. This would explain why some of the tubular polymersomes maintain their structure once internalized by avoiding acidification in the endolysosomal pathway.

A number of studies have demonstrated the ability to form nonspherical nanoparticles.[22,24,44] In particular rod-like nanoparticles and worm-like micelles, otherwise known as filomicelles, have shown promise in drug delivery for their unique targeting abilities and high circulation times.[5,6,45,46] It is now well known that nonspherical nanoparticles have different internalization kinetics when compared to their spherical counterparts, which may be in part due to the large energy requirement for endocytosis of particles with high aspect ratios. In particular, the tangent angle at the point of contact between the particle and cell has been shown to play an important role in whether internalization takes place and upon the rate of internalization.[47−49] Undoubtedly, the impact of shape on internalization will also depend on the size, surface chemistry, and viscoelastic properties of the particle.[47,50]

The average diameter of the tubular polymersomes studied here is around 60 nm (supplementary Figure 3), which is within the optimal diameter range that has been determined theoretically and experimentally to induce nanoparticle endocytosis (reviewed in ref 4). The curvature of the system is therefore ideal for inducing deformation of the plasma membrane around the diameter of the tube. In contrast, the length of the tube is unfavorable for endocytosis. We hypothesize that this interaction, coupled with the high avidity of the PMPC polymer for its receptors, promotes

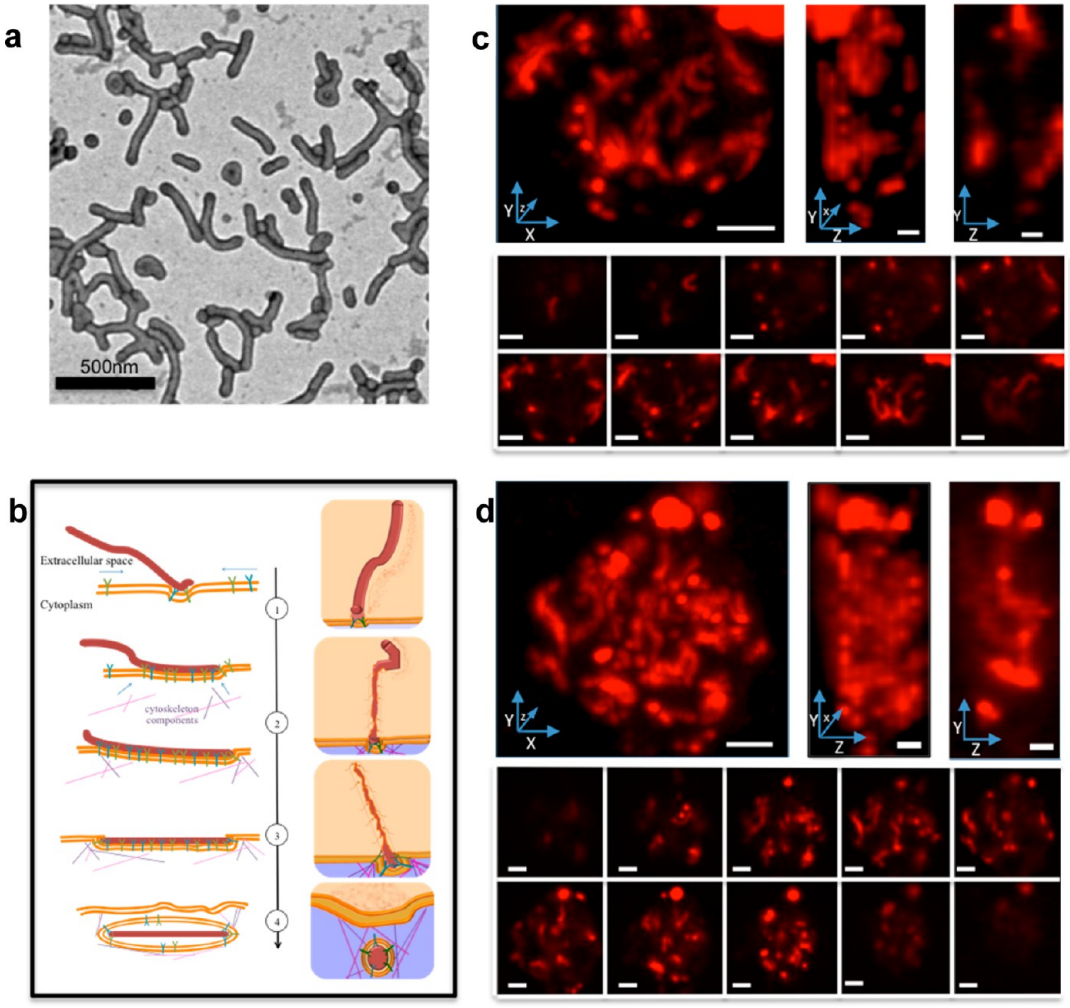

Figure 6. 3D analysis of neutrophils and proposed mechanism of tubular polymersome uptake. (a) TEM micrograph of rhodamine-labeled tubular polymersomes. (b) Illustration demonstrating the proposed internalization mechanism of tubular polymersomes. 3D analysis of confocal *z* stacks of a single neutrophil after 5 h (c) or 9 h (d) treatment with rhodamine-labeled tubular polymersomes. The neutrophils are shown in a three-dimensional view at two angles: straight on (left image) and at 90 deg (central image). The right image shows a single *x* slice through the center of the neutrophil. The lower images in c and d display a montage of the confocal micrographs at the different *z*-planes. Scale bar is 2 μm.

the embedding of the tubular polymersome within the membrane. This strong interaction will cause a local destabilization and deformation of the plasma membrane. This may progress to full endocytosis if components of the cytoskeleton and other molecular endocytic players are recruited to the binding site to assist in the invagination and scission of an endocytic vesicle (Figure 6b). Alternatively, the attached tubes may be slowly internalized from the natural turnover of the plasma membrane. A similar type of delayed or "frustrated" endocytosis has been observed for other highly anisotropic particles.[47,48,51]

Although shape is known to be an important factor in the design of a nanovector, the vast majority of engineered nanovectors are spherical.[52] While worm-like micelles can be formed from amphiphilic block copolymers by controlling the polymer packing parameter,[53] these solid micellular structures do not contain an aqueous core that enables the encapsulation of water-soluble molecules.[54] Carbon nanotubes have received a lot of attention as drug delivery carriers, and although visually carbon nanotubes appear similar in structure to tubular polymersomes, they have very different properties.[4] In contrast to the "soft" polymer membrane, carbon nanotubes are held together by strong covalent bonds, making them stiff and inflexible, and their entry into cells occurs through a "needle-like" penetration of the membrane.[55,56]

The striking effects of polymersome shape on internalization kinetics that were seen in this study immediately highlight opportunities for tubular polymersomes in drug delivery. Despite the large volume of the tubular polymersomes, the internalization rate was surprisingly quick. In particular, the amount of tubular polymersomes internalized into neutrophils after 10 h was similar to the amount of spherical polymersomes of a similar diameter. The larger membrane and

lumenal volumes of tubular polymersomes may allow encapsulation of higher drug loads and give higher delivery efficiencies.

Another intriguing feature of the tubular polymersomes is their long dwelling time at the cell surface before internalization. Particles with high aspect ratios such as tubular polymersomes form more receptor–ligand interactions on the cell surface, leading to an increased binding avidity. However, the increased volume of tubular polymersomes compared with spherical polymersomes results in higher dislodging forces from shear stress.[57,58] This means the ability of a tubular polymersome to bind to a cell in the bloodstream will depend strongly on the affinity of the receptor ligand interaction and the density of receptors on the target cell. Recently the Mitragotri group showed that rod-shaped particles with attached targeting ligands had higher specificity than spherical particles when injected into mice.[6] This is because weak receptor ligand interactions were more easily influenced by shear-induced unbinding.[6] One could speculate that the high membrane dwelling of tubular polymersomes observed in this study may result in an even greater probability of shear-induced detachment. Another possibility is that the shape of the tubular polymersome will influence its intracellular fate, particularly if their length exceeds 500 nm, the typical diameter of a mature endosome; but further work is required to elucidate these features of tubular polymersomes in more detail.

CONCLUSIONS

In conclusion we have demonstrated the formation and purification of tubular polymersomes by film rehydration. The addition of cholesterol or phospholipid was shown to influence the speed and yield of tubular polymersome formation. Finally we showed that the tubular polymersomes have delayed internalization kinetics and are able to encapsulate and deliver fluorescent BSA.

The great potential of filomicelles has been demonstrated through their long circulation times and excellent tumor targeting ability.[5] In this study, we have demonstrated the formation and purification of stable filamentous or tubular polymersomes. The combined shape, versatility, pH sensitivity, and biocompatibility of this nanocarrier will offer novel applications in drug delivery.

METHODS

$PMPC_{25}$–$PDPA_{65}$ was synthesized by reversible addition–fragmentation chain-transfer polymerization (RAFT), and rhodamine 6G-labeled $PMPC_{25}$–$PDPA_{70}$ by atom-transfer radical polymerization (ATRP) as previously described.[59,60] PMPC–PDPA and the desired encapsulate were dissolved in chloroform/methanol (2:1) (10 mg/mL), and the solvent was subsequently evaporated with a desiccator. The resulting polymer film was rehydrated (10 mg/mL in PBS) and exposed to shear stress (magnetic stirring at 200 rpm) for up to 8 weeks. The sample was sonicated for 20 min before analysis (Sonicator Sonicor Instrument Corporation). The formation of particles by the pH switch method was performed as previously described.[13] Cholesterol was purchased from Sigma, and lipid PC was purchased from Avanti Polar lipids.

To visualize thin film dewetting, a film of 10% rhodamine 6G-labeled polymersomes was formed on a coverslip by the same process as above. This coverslip was then placed at a 90° angle to an imaging dish and imaged using a confocal laser scanning microscope (Zeiss LSM Meta) with a 63× oil immersion lens. At time 0 PBS was added to the imaging dish, and the film was left stirring with a magnetic stirrer until imaging at the time points highlighted. For TEM studies polymersomes were adsorbed onto glow discharged copper grids (Agar Scientific) and stained with 0.75 wt % phosphotungstic acid (PTA) aqueous solution [pH 7.4] followed by imaging with a FEI Tecnai G2 Spirit electron microscope.

Polymersomes were centrifuged at 2000 RCF for 20 min, the supernatant was removed, and the resulting pellet was resuspended in a volume of PBS equal to the original volume. The procedure was then repeated at 15 000 RCF. HPLC analysis was performed on a Dionex Ultimate 3000 system, using a C_{18} analytical column (Phenomenex Jupiter; 300A, 150 × 4.6 mm, 5 μm). For quantification of the cholesterol-loaded polymersomes a multistep gradient of methanol (MeOH) (0.1% trifluoroacetic acid (TFA)) in Milli-Q filtered H_2O (MQ) (0.1% TFA) was used: 0 min 30%, 5 min 30%, 12 min 100%, 20 min 100%, 21 min 30%, 23 min 30%; for PC the multistep gradient was as follows: 0 min 5%, 7 min 5%, 9 min 100%, 13 min 100%, 15 min 5%, 20 min 5%. DLS measurements were performed on a Zetasizer Nano ZS (Malvern Ltd.) at a copolymer concentration of 0.25 mg/mL as previously described.[59]

To analyze the morphology of tubular polymersomes, multiple TEM micrographs with at least 500 tubular polymersomes from each group were analyzed from multiple TEM grids. Persistent length (*i.e.*, the longest single tubular length) and total length (the length of all branches combined) were measured manually. In addition the number of branches for each particle was noted, and the cross sectional area was measured. Using the total length and the cross sectional area of the tube the average diameter was calculated by assuming that a tube cross section consisted of a rectangle of length L and width D and two half -circle end-caps of diameter D. Using the diameter and total length of the tube the number of chains (N(agg)) was calculated based on a membrane thickness of 7 nm and a density calculated previously.[17] Each tubular polymersome was assumed to consist of a hollow cylinder of measured diameter D and measured length L with two end-cap half-spherical vesicles of diameter D. The N(agg) was calculated for each tubular polymersome by dividing the total calculated membrane volume by the volume of PDPA.

Neutrophils were isolated from fresh venous blood taken from healthy donors using density separation with a Percoll gradient as described previously.[61] FaDu cells were purchased from American Type Culture Collection (Manassas, VA, USA) and cultured in standard cell culture medium. For flow cytometry experiments FaDu cells were seeded in 24-well plates and allowed to grow for 1 day before incubating with polymersomes. After incubation with 10% rhodamine-labeled tubular or spherical polymersomes for the specified time periods, neutrophils were centrifuged at 3000 rpm for 3 min and washed with PBS, then left on ice until analysis. FaDu cells were washed with PBS, trypsinized, centrifuged at 2000 rpm, and then resuspended in cold PBS before analysis. Flow cytometry was done on a BD LSR II flow cytometer with the 488 nm laser. The MFI was calculated by normalizing the median fluorescence intensity of polymersome-treated cells by cells treated only with PBS (negative control). This value was then divided by the mass

per particle. The mass per particle was calculated by dividing the mass of polymer added to the cells by the number of particles calculated from the sum of the molar mass of each particle multiplied by Avogadro's number, divided by the *N*(agg) of the particle.

Polymersomes of 60 and 240 nm were purified from spherical polymersomes made by the pH switch method. Small particles were first removed using the KrosFlo Research II*i* tangential flow filtration system with a 50 nm hollow fiber. Centrifuging the polymersomes at 5000 RCF and discarding the pellet removed large particles. The 240 nm polymersomes were then extracted by centrifuging the polymersomes at 10 000 RCF and rehydrating the pellet in PBS. The supernatant was then recentrifuged at 20 000 RCF for 20 min, and the resulting supernatant was extracted. This fraction contained the polymersomes with an average diameter of 60 nm. Size measurements were assessed by DLS.

For imaging experiments FaDu cells were seeded in 35 mm μ-dishes for microscopy, purchased from Ibidi 24 h prior to incubation. Neutrophils or FaDu cells were incubated with 70% PMPC–PDPA, 30% rhodamine 6G-labeled PMPC–PDPA for 5 or 9 h. The cells were then washed as above, neutrophils were then left to settle on the μ-dish for 30 min, and the cells were imaged live using a PerkinElmer UltraVIEW VoX spinning disk confocal microscope with a 60× oil immersion lens and a *z* thickness of 1 μm. In a parallel experiment neutrophils and FaDu cells were seeded as before and treated for 9 h with tubular polymersomes encapsulating AlexaFluor647-BSA (conjugated using the commercially available antibody labeling kit (Invitrogen)) at a final concentration of 0.5 mg/mL of polymer. The BSA was encapsulated by electroporation as described previously.[43] The cells were imaged live using a PerkinElmer UltraVIEW VoX spinning disk confocal microscope with a 60× oil immersion lens and a *z* thickness of 1 μm.

Conflict of Interest: The authors declare no competing financial interest.

Acknowledgment. The authors thank Biocompatibles UK Ltd. for supplying the PDPA monomer and Prof. S. Armes and Drs. J. Madsen and N. Warren for the synthesis of the PMPC–PDPA copolymers as well as the useful discussion and critical reading of the manuscript. J.D.R. and G.Y. thank the MRC, M.A.O. thanks the BBSRC, and L.C. thanks Biocompatibles Ltd. for supporting their Ph.D. scholarships. O.B. is supported by Parkinson's UK (G1202), S.A.R. is supported by an MRC Senior Clinical Fellowship, and G.B. holds an ERC-STG Award (MEVIC). Finally the authors thank Silvia Bianco for the design and creation of the abstract graphic.

Supporting Information Available: SAXS patterns and further TEM, HPLC, DLS, and confocal microscopy. This material is available free of charge *via* the Internet at http://pubs.acs.org.

REFERENCES AND NOTES

1. Akinc, A.; Battaglia, G. Exploiting Endocytosis for Nanomedicines. *Cold Spring Harbor Perspect. Bio.* **2013**, *5*, 16980–16980.
2. Duncan, R.; Richardson, S. C. W. Endocytosis and Intracellular Trafficking as Gateways for Nanomedicine Delivery: Opportunities and Challenges. *Mol. Pharmaceutics* **2012**, *9*, 2380–2402.
3. Rajendran, L.; Knoelker, H.-J.; Simons, K. Subcellular Targeting Strategies for Drug Design and Delivery. *Nat. Rev. Drug Discovery* **2010**, *9*, 29–42.
4. Canton, I.; Battaglia, G. Endocytosis at the Nanoscale. *Chem. Soc. Rev.* **2012**, *41*, 2718–2739.
5. Geng, Y.; Dalhaimer, P.; Cai, S.; Tsai, R.; Tewari, M.; Minko, T.; Discher, D. E. Shape Effects of Filaments *versus* Spherical Particles in Flow and Drug Delivery. *Nat. Nanotechnol.* **2007**, *2*, 249–255.
6. Kolhar, P.; Anselmo, A. C.; Gupta, V.; Pant, K.; Prabhakarpandian, B.; Ruoslahti, E.; Mitragotri, S. Using Shape Effects to Target Antibody-Coated Nanoparticles to Lung and Brain Endothelium. *Proc. Natl. Acad. Sci. U.S.A.* **2013**, *110*, 10753–10758.
7. Albanese, A.; Tang, P. S.; Chan, W. C. W. The Effect of Nanoparticle Size, Shape, and Surface Chemistry on Biological Systems. *Annu. Rev. Biomed. Eng.* **2012**, *14*, 1–16.
8. Chithrani, B. D.; Ghazani, A. A.; Chan, W. C. W. Determining the Size and Shape Dependence of Gold Nanoparticle Uptake into Mammalian Cells. *Nano Lett.* **2006**, *6*, 662–668.
9. Gratton, S. E. A.; Ropp, P. A.; Pohlhaus, P. D.; Luft, J. C.; Madden, V. J.; Napier, M. E.; DeSimone, J. M. The Effect of Particle Design on Cellular Internalization Pathways. *Proc. Natl. Acad. Sci. U.S.A.* **2008**, *105*, 11613–11618.
10. Massignani, M.; Canton, I.; Sun, T.; Hearnden, V.; MacNeil, S.; Blanazs, A.; Armes, S. P.; Lewis, A.; Battaglia, G. Enhanced Fluorescence Imaging of Live Cells by Effective Cytosolic Delivery of Probes. *PLoS One* **2010**, *5*, 10459.
11. Lomas, H.; Canton, I.; MacNeil, S.; Du, J.; Armes, S. P.; Ryan, A. J.; Lewis, A. L.; Battaglia, G. Biomimetic pH Sensitive Polymersomes for Efficient DNA Encapsulation and Delivery. *Adv. Mater.* **2007**, *19*, 4238–4243.
12. Murakami, T.; Sunada, Y. Plasmid DNA Gene Therapy by Electroporation: Principles and Recent Advances. *Curr. Gene Ther.* **2011**, *11*, 447–456.
13. Canton, I.; Massignani, M.; Patikarnmonthon, N.; Chierico, L.; Robertson, J.; Renshaw, S. A.; Warren, N. J.; Madsen, J. P.; Armes, S. P.; Lewis, A. L.; *et al.* Fully Synthetic Polymer Vesicles for Intracellular Delivery of Antibodies in Live Cells. *FASEB J.* **2013**, *27*, 98–108.
14. Pegoraro, C.; Cecchin, D.; Gracia, L. S.; Warren, N.; Madsen, J.; Armes, S. P.; Lewis, A.; MacNeil, S.; Battaglia, G. Enhanced Drug Delivery to Melanoma Cells Using PMPC-PDPA Polymersomes. *Cancer Lett.* **2013**, *334*, 328–337.
15. Wayakanon, K.; Thornhill, M. H.; Douglas, C. W. I.; Lewis, A. L.; Warren, N. J.; Pinnock, A.; Armes, S. P.; Battaglia, G.; Murdoch, C. Polymersome-Mediated Intracellular Delivery of Antibiotics to Treat Porphyromonas Gingivalis-Infected Oral Epithelial Cells. *FASEB J.* **2013**, *27*, 4455–4465.
16. Madsen, J.; Canton, I.; Warren, N. J.; Themistou, E.; Blanazs, A.; Ustbas, B.; Tian, X.; Pearson, R.; Battaglia, G.; Lewis; *et al.* Nile Blue-Based Nanosized pH Sensors for Simultaneous Far-Red and Near-Infrared Live Bioimaging. *J. Am. Chem. Soc.* **2013**, *135*, 14863–14870.
17. Massignani, M.; LoPresti, C.; Blanazs, A.; Madsen, J.; Armes, S. P.; Lewis, A. L.; Battaglia, G. Controlling Cellular Uptake by Surface Chemistry, Size, and Surface Topology at the Nanoscale. *Small* **2009**, *5*, 2424–2432.
18. Smart, T.; Lomas, H.; Massignani, M.; Flores-Merino, M. V.; Perez, L. R.; Battaglia, G. Block Copolymer Nanostructures. *Nano Today* **2008**, *3*, 38–46.
19. Dimova, R.; Seifert, U.; Pouligny, B.; Forster, S.; Dobereiner, H. G. Hyperviscous Diblock Copolymer Vesicles. *Eur. Phys. J. E: Soft Matter Biol. Phys.* **2002**, *7*, 241–250.
20. Battaglia, G.; Tomas, S.; Ryan, A. J. Lamellarsomes: Metastable Polymeric Multilamellar Aggregates. *Soft Matter* **2007**, *3*, 470–475.
21. Battaglia, G.; Ryan, A. J. Pathways of Polymeric Vesicle Formation. *J. Phys. Chem. B* **2006**, *110*, 10272–10279.
22. Grumelard, J.; Taubert, A.; Meier, W. Soft Nanotubes from Amphiphilic ABA Triblock Macromonomers. *Chem. Commun.* **2004**, 1462–1463.
23. Stewart, S.; Liu, G. Block Copolymer Nanotubes. *Angew. Chem.* **2000**, *112*, 348–352.
24. Reiner, J. E.; Wells, J. M.; Kishore, R. B.; Pfefferkorn, C.; Helmerson, K. Stable and Robust Polymer Nanotubes Stretched from Polymersomes. *Proc. Natl. Acad. Sci. U.S.A.* **2006**, *103*, 1173–1177.
25. Yu, K.; Eisenberg, A. Bilayer Morphologies of Self-Assembled Crew-Cut Aggregates of Amphiphilic PS-b-PEO Diblock Copolymers in Solution. *Macromolecules* **1998**, *31*, 3509–3518.
26. van Oers, M. C. M.; Rutjes, F.; van Hest, J. C. M. Tubular Polymersomes: A Cross-Linker-Induced Shape Transformation. *J. Am. Chem. Soc.* **2013**, *135*, 16308–16311.
27. Lomas, H.; Massignani, M.; Abdullah, K. A.; Canton, I.; Lo Presti, C.; MacNeil, S.; Du, J.; Blanazs, A.; Madsen, J.; Armes, S. P.; *et al.* Non-Cytotoxic Polymer Vesicles for Rapid and

Efficient Intracellular Delivery. *Faraday Discuss.* **2008**, *139*, 143–159.
28. Limary, R.; Green, P. F. Dewetting Instabilities in Thin Block Copolymer Films: Nucleation and Growth. *Langmuir* **1999**, *15*, 5617–5622.
29. Battaglia, G.; Ryan, A. J. Neuron-Like Tubular Membranes made of Diblock Copolymer Amphiphiles. *Angew. Chem.* **2006**, *45*, 2052–2056.
30. Green, P. F.; Limary, R. Block Copolymer Thin Films: Pattern Formation and Phase Behavior. *Adv. Colloid Interface Sci.* **2001**, *94*, 53–81.
31. Sharma, A.; Khanna, R. Pattern Formation in Unstable Thin Liquid Films. *Phys. Rev. Lett.* **1998**, *81*, 3463–3466.
32. LoPresti, C.; Lomas, H.; Massignani, M.; Smart, T.; Battaglia, G. Polymersomes: Nature Inspired Nanometer Sized Compartments. *J. Mater. Chem.* **2009**, *19*, 3576–3590.
33. Battaglia, G.; Ryan, A. J. The Evolution of Vesicles from Bulk Lamellar Gels. *Nat. Mater.* **2005**, *4*, 869–876.
34. Lipowsky, R.; Leibler, S. Unbinding Transitions of Interacting Membranes. *Phys. Rev. Lett.* **1986**, *56*, 2541–2544.
35. Helfrich, W. Lyotropic Lamellar Phases. *J. Phys.: Condens. Matter* **1994**, *6*, A79–A92.
36. McMullen, T. P. W.; Lewis, R.; McElhaney, R. N. Cholesterol-Phospholipid Interactions, the Liquid-Ordered Phase and Lipid Rafts in Model and Biological Membranes. *Curr. Opin. Colloid Interface Sci.* **2004**, *8*, 459–468.
37. Sugar, I. P.; Chong, P. L. G. A Statistical Mechanical Model of Cholesterol/Phospholipid Mixtures: Linking Condensed Complexes, Superlattices, and the Phase Diagram. *J. Am. Chem. Soc.* **2012**, *134*, 1164–1171.
38. Nam, J.; Vanderlick, T. K.; Beales, P. A. Formation and Dissolution of Phospholipid Domains with Varying Textures in Hybrid Lipo-Polymersomes. *Soft Matter* **2012**, *8*, 7982–7988.
39. Nam, J.; Beales, P. A.; Vanderlick, T. K. Giant Phospholipid/Block Copolymer Hybrid Vesicles: Mixing Behavior and Domain Formation. *Langmuir* **2011**, *27*, 1–6.
40. Winzen, S.; Bernhardt, M.; Schaeffel, D.; Koch, A.; Kappl, M.; Koynov, K.; Landfester, K.; Kroeger, A. Submicron Hybrid Vesicles Consisting of Polymer-Lipid and Polymer-Cholesterol Blends. *Soft Matter* **2013**, *9*, 5883–5890.
41. Moon, J. J.; Huang, B.; Irvine, D. J. Engineering Nano- and Microparticles to Tune Immunity. *Adv. Mater.* **2012**, *24*, 3724–3746.
42. Peer, D.; Karp, J. M.; Hong, S.; FaroKhzad, O. C.; Margalit, R.; Langer, R. Nanocarriers as an Emerging Platform for Cancer Therapy. *Nat. Nanotechnol.* **2007**, *2*, 751–760.
43. Wang, L.; Chierico, L.; Little, D.; Patikarnmonthon, N.; Yang, Z.; Azzouz, M.; Madsen, J.; Armes, S. P.; Battaglia, G. Encapsulation of Biomacromolecules within Polymersomes by Electroporation. *Angew. Chem.* **2012**, *51*, 11122–11125.
44. Mitragotri, S.; Lahann, J. Physical Approaches to Biomaterial Design. *Nat. Mater.* **2009**, *8*, 15–23.
45. Cai, S. S.; Vijayan, K.; Cheng, D.; Lima, E. M.; Discher, D. E. Micelles of Different Morphologies - Advantages of Worm-like Filomicelles of PEO-PCL in Paclitaxel Delivery. *Pharm. Res.* **2007**, *24*, 2099–2109.
46. Christian, D. A.; Cai, S. S.; Garbuzenko, O. B.; Harada, T.; Zajac, A. L.; Minko, T.; Discher, D. E. Flexible Filaments for in *Vivo* Imaging and Delivery: Persistent Circulation of Filomicelles Opens the Dosage Window for Sustained Tumor Shrinkage. *Mol. Pharmaceutics* **2009**, *6*, 1343–1352.
47. Decuzzi, P.; Ferrari, M. The Receptor-Mediated Endocytosis of Nonspherical Particles. *Biophys. J.* **2008**, *94*, 3790–3797.
48. Champion, J. A.; Mitragotri, S. Role of Target Geometry in Phagocytosis. *Proc. Natl. Acad. Sci. U.S.A.* **2006**, *103*, 4930–4934.
49. Gratton, S. E. A.; Napier, M. E.; Ropp, P. A.; Tian, S.; DeSimone, J. M. Microfabricated Particles for Engineered Drug Therapies: Elucidation into the Mechanisms of Cellular Internalization of PRINT Particles. *Pharm. Res.* **2008**, *25*, 2845–2852.
50. Decuzzi, P.; Lee, S.; Decuzzi, M.; Ferrari, M. Adhesion of Microfabricated Particles on Vascular Endothelium: A Parametric Analysis. *Ann. Biomed. Eng.* **2004**, *32*, 793–802.
51. Champion, J. A.; Mitragotri, S. Shape Induced Inhibition of Phagocytosis of Polymer Particles. *Pharm. Res.* **2009**, *26*, 244–249.
52. Robertson, J. D.; Patikarnmonthon, N.; Joseph, A. S.; Battaglia, G. Block Copolymer Micelles and Vesicles for Drug Delivery. In *Engineering Polymer Systems for Improved Drug Delivery*; Bader, R. A., Putnam, D. A., Eds.; John Wiley & Sons, 2014; pp 163−183.
53. Israelachvili, J. N.; Mitchell, D. J.; Ninham, B. W. Theory of Self-Assembly of Hydrocarbon Amphiphiles into Micelles and Bilayers. *J. Chem. Soc., Faraday Trans.* **1976**, *72*, 1525–1568.
54. Blanazs, A.; Armes, S. P.; Ryan, A. J. Self-Assembled Block Copolymer Aggregates: From Micelles to Vesicles and their Biological Applications. *Macromol. Rapid Commun.* **2009**, *30*, 267–277.
55. Kostarelos, K.; Lacerda, L.; Pastorin, G.; Wu, W.; Wieckowski, S.; Luangsivilay, J.; Godefroy, S.; Pantarotto, D.; Briand, J. P.; Muller, S.; Prato, M.; Bianco, A. Cellular Uptake of Functionalized Carbon Nanotubes Is Independent of Functional Group and Cell Type. *Nat. Nanotechnol.* **2007**, *2*, 108–113.
56. Porter, A. E.; Gass, M.; Muller, K.; Skepper, J. N.; Midgley, P. A.; Welland, M. Direct Imaging of Single-Walled Carbon Nanotubes in Cells. *Nat. Nanotechnol.* **2007**, *2*, 713–717.
57. Decuzzi, P.; Ferrari, M. The Adhesive Strength of Non-spherical Particles Mediated by Specific Interactions. *Biomaterials* **2006**, *27*, 5307–5314.
58. Lee, S. Y.; Ferrari, M.; Decuzzi, P. Shaping Nano-/Microparticles for Enhanced Vascular Interaction in Laminar Flows. *Nanotechnology* **2009**, *20*, 495101.
59. Pearson, R. T.; Warren, N. J.; Lewis, A. L.; Armes, S. P.; Battaglia, G. Effect of pH and Temperature on PMPC-PDPA Copolymer Self-Assembly. *Macromolecules* **2013**, *46*, 1400–1407.
60. Madsen, J.; Warren, N. J.; Armes, S. P.; Lewis, A. L. Synthesis of Rhodamine 6G-Based Compounds for the ATRP Synthesis of Fluorescently Labeled Biocompatible Polymers. *Biomacromolecules* **2011**, *12*, 2225–2234.
61. Haslett, C.; Guthrie, L. A.; Kopaniak, M. M.; Johnston, R. B.; Henson, P. M. Modulation of Multiple Neutrophil Functions by Preparative Methods or Trace Concentrations of Bacterial Lipopolysacaride. *Am. J. Pathol.* **1985**, *119*, 101–110.